Microporous and Mesoporous Materials 269 (2018) 93–96

Contents lists available at ScienceDirect

Microporous and Mesoporous Materials

journal homepage: www.elsevier.com/locate/micromeso

Towards clinically feasible relaxation-diffusion correlation MRI using MADCO

Dan Benjamini*, Peter J. Basser

Quantitative Imaging and Tissue Sciences, NICHD, National Institutes of Health, Bethesda, MD, 20892, USA

ARTICLE INFO

Article history:
Received 10 November 2016
Received in revised form
7 January 2017
Accepted 1 February 2017
Available online 5 February 2017

Keywords:
Fredholm integral
Inverse problems
Relaxometry
Diffusometry
Relaxation-diffusion
Multidimensional
Distribution
NMR
MRI

ABSTRACT

Multidimensional relaxation-diffusion correlation (REDCO) NMR is an assumption-free method that measures how water is distributed within materials. Although highly informative, REDCO had never been used in clinical MRI applications because of the large amount of data it requires, leading to infeasible scan times. A recently suggested novel experimental design and processing framework, marginal distributions constrained optimization (MADCO), was used here to accelerate and improve the reconstruction of such MRI correlations. MADCO uses the 1D marginal distributions as *a priori* information, which provide powerful constraints when 2D spectra are reconstructed, while their estimation requires an order of magnitude less data than conventional 2D approaches. In this work we experimentally examined the impact the complexity of the correlation distribution has on the accuracy and robustness of the estimates. MADCO and a conventional method were compared using two T_1–D phantoms that differ in the proximity of their peaks, leading to a relatively simple case as opposed to a more challenging one. The phantoms were used to vet the achievable data compression using MADCO under these conditions. MADCO required ~43 and ~30 less data than the conventional approach for the simple and complex spectra, respectively, making it potentially feasible for preclinical and even clinical applications.

Published by Elsevier Inc.

1. Introduction

Properties such as T_1 and T_2 time constants, and diffusivity (D), are determined by the physical barriers and chemical environments of water residing within materials. Multidimensional NMR methods can be used to measure how these properties are correlated (e.g., T_1–D, T_1–T_2), and from them identify and characterize microstructure-related water dynamics in many applications [1,2]. To obtain this information one has to solve an inverse problem – the Fredholm integral of the first kind [3]. In most 2D NMR applications, the part that relates the experimental and the measured variables (e.g., T_1 and inversion time, τ, or D and diffusion weighting, b, see Experimental) is called the kernel, and has an exponential form. In this case solving the Fredholm integral is reduced to a 2D inverse Laplace transform (ILT), which is a classic ill-conditioned problem [4]. Traditionally, acquiring large amounts of data are required to solve it. The most common and efficient 2D-ILT algorithm [5] is typically used in 2D NMR applications to compress the signal without losing useful information, revealing a redundancy in some basis representations.

Although multidimensional relaxation-diffusion correlation (REDCO) MRI methods have the potential to provide valuable biological information regarding the underlying microscopic structure of the tissue, preclinical and clinical applications are infeasible owing to long acquisition times. To migrate REDCO MRI methods to measure *in vivo* mean cell volume, cell types distribution, and water exchange between compartments and cells, the required number of MR acquisitions must be vastly reduced. Taking a step in this direction, compressed sensing was used as a more efficient data sampling strategy [6], able to achieve an acceleration factor of 4–10, depending on the complexity of the spectrum. This acceleration however, was not sufficient for preclinical and clinical MRI applications.

A novel experimental design and reconstruction framework that might achieves suitable compression was recently introduced [7]. The concept in this approach is to use the more accessible 1D information (e.g., T_1 distribution) to enforce physical constraints on the multidimensional distribution. For example, given a 2D joint distribution of T_1–D, the marginal distribution of D is simply the probability distribution of D averaging over all T_1 values. This is

* Corresponding author.
E-mail address: dan.benjamini@nih.gov (D. Benjamini).

http://dx.doi.org/10.1016/j.micromeso.2017.02.001
1387-1811/Published by Elsevier Inc.

typically calculated by summing or integrating the joint probability distribution over T_1. The 1D distributions therefore contain information regarding their joint distribution, which should be exploited [8]. This method, the marginal distribution constrained optimization (MADCO), reduces the amount of required data by selectively sampling the experimental parameters space. Following the above example, instead of sampling the entire experimental parameters space (τ, b) and from it estimate the 2D distribution $\mathscr{F}(T_1, D)$ (Fig. 1A), using MADCO would only require sampling along τ and b axes (i.e., 1D data), complemented with a small number of acquisitions in the 2D space (Fig. 1B). The 2D reconstruction would then have two steps: (1) estimate $\mathscr{F}(T_1)$ and $\mathscr{F}(D)$ from the 1D data, and then (2) use these 1D spectra to constrain the estimation of $\mathscr{F}(T_1, D)$ from the remaining 2D data.

Using MADCO on simulated data revealed that the extent of achievable compression depends on the complexity of the estimated spectrum [7]. In this work we extend this investigation and experimentally examine the impact the complexity of the 2D spectra has on the accuracy and robustness of the estimates. Although the method is equally applicable to other types of multidimensional experiments, we compared MADCO and a conventional approach using two T_1–D phantoms. Both phantoms have two peaks in the T_1–D space, however they differ in the proximity of those peaks, leading to a relatively simple case as opposed to a more challenging one.

2. Experimental

Doped water and polyvinylpyrrolidone (PVP) (Sigma-Aldrich, K value 29–32) were used to create two T_1–D phantoms, phantom A and phantom B, each with two distinct peaks. Increasing PVP w/v concentration is negatively correlated with both the diffusivity and T_1, allowing for a range of T_1–D values. Phantom A consisted of two solutions: (1) purified water with 0.5 mM gadopentetate dimeglumine (Magnevist, Bayer, Germany), and (2) 35% w/v PVP purified water with 0.18 mM Magnevist. Phantom B consisted of two solutions: (1) 35% w/v PVP purified water with 0.18 mM Magnevist, and (2) 20% w/v PVP purified water with 0.5 mM Magnevist. The corresponding weighted geometric means (gm) of the relaxation times and diffusivities (gmT_1, gm$D$), as measured separately for each sample (see Methods) are shown in Fig. 3. Each solution was placed in a 4 mm NMR tube; these were then inserted together into a 15 mm NMR tube.

Images were collected on a 7 T Bruker wide-bore vertical magnet with an AVANCE III MRI spectrometer equipped with a Micro 2.5 microimaging probe. MRI data were acquired with an inversion recovery spin-echo diffusion-weighted echo planar imaging (IR–DWI–EPI) sequence, with an adiabatic 180° inversion pulse applied before the standard spin-echo diffusion weighted sequence (Fig. 2). The full 2D experimental set had 40 diffusion gradient linear steps (G) ranging from 0 to 900 mT/m, 38 inversion times (τ) with logarithmic temporal spacing ranging from 100 to 3000 ms, and an additional magnetization equilibrium scan with an inversion time of 10 s. Other acquisition parameters were diffusion gradient duration and separation of $\delta = 3$ ms and $\Delta = 15$ ms, respectively, leading to a b-value range of 0–6000 s/mm^2 ($b = \gamma^2\delta^2G^2(\Delta - \delta/3)$, where γ is the gyromagnetic ratio), TE = 50 ms, and TR = inversion time + 10 s. A single 5 mm axial slice with a matrix size and resolution of 64×64 and 0.2×0.2 mm^2, respectively, acquired with 2 averages and 4 segments. The experimental signal-to-noise ratio (SNR) in the full 2D experiment was ~700.

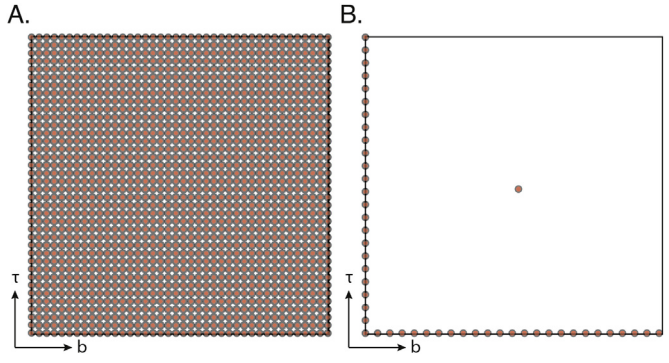

Fig. 1. Schematic illustration of the experimental designs used to obtain a 2D correlation function, $\mathscr{F}(T_1, D)$. (A) The conventinal approach, in which the 2D experimental parameter space is uniformly and densely sampled. (B) MADCO acquisition strategy, in which sampling of 1D data is performed prior to a small number of acquisitions in the 2D space.

3. Methods

The following expression [3] describes the signal attenuation from 2D NMR experiments with separable T_1 and D kernels:

$$M(\tau, b) = \int\int \mathscr{F}(T_1, D)\, k_1(\tau, T_1) k_2(b, D)\, \mathrm{d}T_1\, \mathrm{d}D, \tag{1}$$

Eq. (1) can be discretized on a grid with $N_{T_1} = N_D = 50$ values of T_1 and D, respectively, and have the general form of

$$M(\tau, b) = \sum_{n=1}^{N_{T_1}} \sum_{m=1}^{N_D} \mathbf{F}(T_{1,n}, D_m) \exp\left(-\frac{\tau}{T_{1,n}}\right) \exp(-bD_m), \tag{2}$$

while it is worth noting that for T_1-weighted measurements the fully recovered data are subtracted from the data set to remove signal offset.

The matrices $K_1 = \exp(-\tau/T_{1,n})$ and $K_2 = \exp(-bD_m)$, and F are discretized version of k_1, k_2, and $\mathscr{F}$, respectively, and Eq. (2) can be written in matrix form as

$$M = K_1 F K_2', \tag{3}$$

As discussed earlier, Eq. (3) represents an ill-conditioned problem, i.e., a small change in M may result in large variations in F. A standard approach to solving ill-conditioned problems is to regularize them. When the spectrum is expected to be smooth, ℓ_2 regularization is appropriate [9]. However, in the case of the phantom, the T_1–D space is comprised of discrete components, therefore making ℓ_1 regularization a more suitable choice since it has many of the beneficial properties of ℓ_2 regularization, but yields sparse models [10]. The regularized problem considered in this study was

$$F^{(\alpha)} = \underset{F \geq 0}{\operatorname{argmin}} \left(||K_1 F K_2' - M||_2^2 + \alpha ||F||_1^2 \right), \tag{4}$$

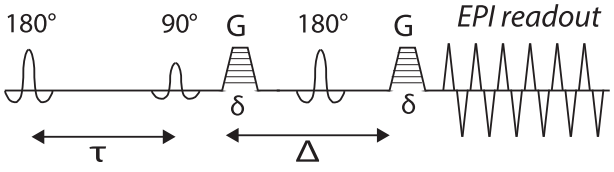

Fig. 2. The IR–DWI–EPI sequence. The full 2D experimental set had 40 diffusion gradient linear steps, G, and 38 inversion times, τ, with logarithmic spacing.

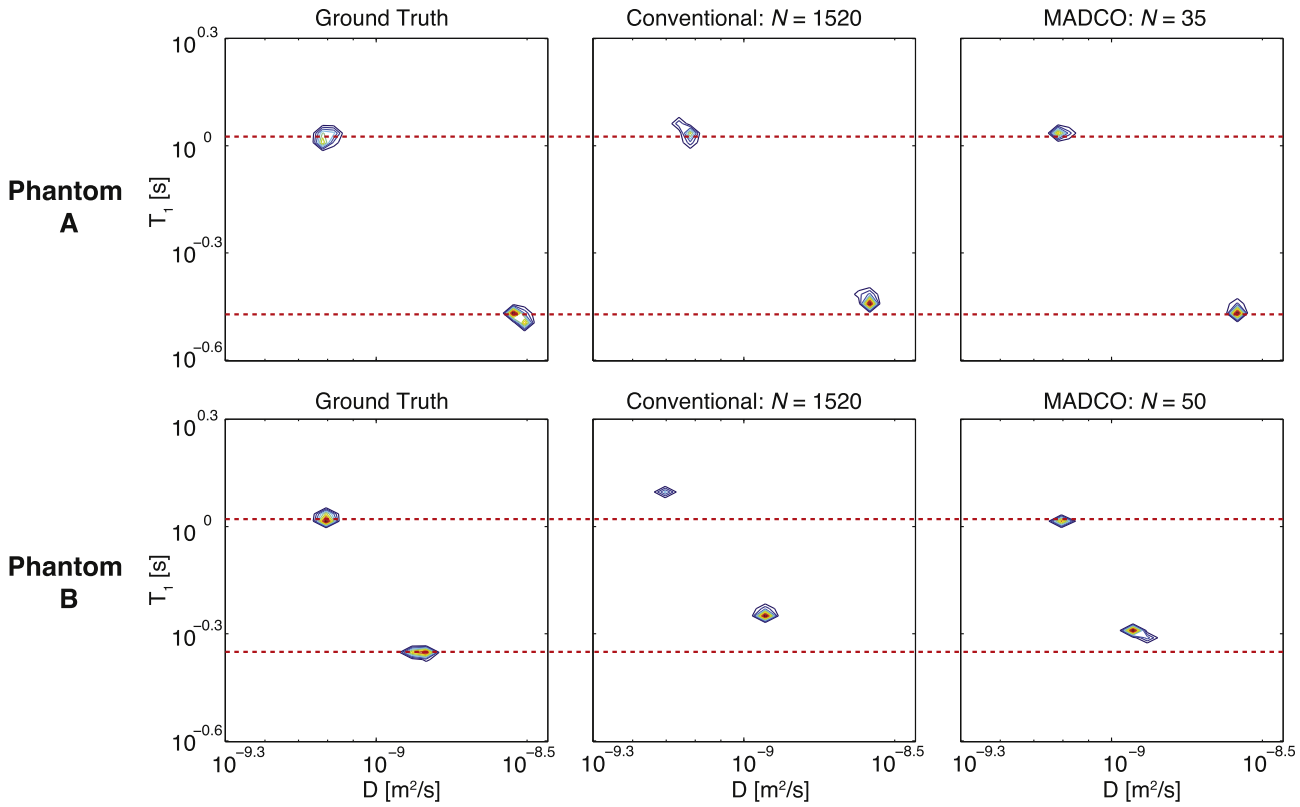

Fig. 3. T_1–D phantom spectra reconstruction using the two methods. Results from phantom A and B presented in the top and bottom rows, respectively. Left to right: ground truth, conventional approach using the full data set, and MADCO. Ground truth (gmT_1, gm$D$) peaks are: phantom A – (0.33 s, 2.0×10^{-9} m^2/s), (1.05 s, 7.90×10^{-10} m^2/s), phantom B – (0.44 s, 1.23×10^{-9} m^2/s), (1.05 s, 7.93×10^{-10} m^2/s).

where $\|\cdots\|_i$ are the ℓ_1 and ℓ_2 norms, for $i = 1, 2$, respectively. The regularization parameter, α, was chosen based on the S-curve method [9], which uses the fit error, $\chi(\alpha) = \|K_1 F^{(\alpha)} K_2' - M\|_2$. The regularization parameter was determined such that $\mathrm{d}(\log\chi)/\mathrm{d}(\log\alpha) = \mathrm{TOL}$, with $\mathrm{TOL} = 0.1$ [9].

Eq. (4) with the standard nonnegativity constraints represents the conventional approach to estimating 2D NMR spectra [5]. To vastly reduce the number of needed data points while conserving the accuracy of the estimates, the MADCO approach includes, in addition, the following inequality constraints when solving Eq. (4) [7]:

$$\left\| \sum_{n=1}^{N_D} \mathbf{F}(T_1, D_n) - F(T_1) \right\|_2 < \sigma_1 \tag{5}$$

and

$$\left\| \sum_{n=1}^{N_{T_1}} \mathbf{F}(T_{1,n}, D) - F(D) \right\|_2 < \sigma_2. \tag{6}$$

where in this work we set $\sigma_1 = \sigma_2$ as the standard deviation of the noise (as determined after complete signal decay) normalized by the unattenuated signal and N_{T_1}. These inequality constraints are in fact a relaxed version of the equality constraints that should be applied, since in an idealized system $\sum_{n=1}^{N_D} \mathbf{F}(T_1, D_n) = F(T_1)$ and $\sum_{n=1}^{N_{T_1}} \mathbf{F}(T_{1,n}, D) = F(D)$. Like the nonnegativity constraints, these also represent physical conditions that must be fulfilled – "conservation of mass" of the 2D probability distribution projected onto one of its axes – and can be applied in a similar manner. The advantage of using the constraints in Eqs. (5) and (6) is in the estimation of the marginal 1D distributions, $F(T_1)$ and $F(D)$, which requires only two 1D experiments, with substantially less data acquired. Using MADCO will be shown here to dramatically reduce the number of acquisitions required to estimate the 2D distribution, compared to the conventional approach.

Ground truth was established thanks to the spatially resolved acquired data. Imaging the PVP phantoms enabled separate analysis of each of the T_1–D peaks in each of the phantoms. By selecting separate regions of interest (ROI) the signal attenuation from each peak was isolated, and solving Eq. (4) resulted in the spectra of single peak data (i.e., well-posed monoexponential). The 2D distributions obtained from these analyses were averaged according to their relative spin density and taken as the ground truth.

Performance of the proposed method was assessed by computing the difference between the estimated and ground truth distributions. The Jensen distance, which is a well-established method of measuring the divergence between two probability distributions [11], was used. This quantity is a metric, and is a symmetric version of the Kullback-Leibler divergence, bounded by 0 and 1, and defined for two distributions, Q and P, as

$$d_{JD} = \sum_i \left[\frac{P_i \ln(P_i) + Q_i \ln(Q_i)}{2} - \left(\frac{P_i + Q_i}{2} \right) \ln\left(\frac{P_i + Q_i}{2} \right) \right]. \tag{7}$$

4. Results and discussion

The difference between the two phantoms, A and B, is in the difficulty to resolve their T_1–D peaks. In phantom A (Ground Truth,

top row of Fig. 3), the peaks are more separated, with a ratio of the T_1 relaxation times and diffusivities of approximately 3.2 and 2.5, respectively. In the more challenging phantom B (Ground Truth, bottom row of Fig. 3), the ratio of the T_1 relaxation times and the diffusivities were approximately 2.4 and 1.5, respectively. The accuracy was tested with both phantoms, using the conventional approach with the full data, i.e., $N = 1520$ acquisitions, contrasted with using MADCO to obtain the spectra. In the latter case, the minimal number of acquisitions that resulted in an accurate $T_1{-}D$ spectrum reconstruction was used.

The $T_1{-}D$ distributions corresponding to phantom A are shown in the top row of Fig. 3. For this simpler phantom, the spectrum obtained from using the conventional approach with the full data set was in good agreement with the ground truth, resulting in geometric mean peaks of $(0.31\,s,\ 2.07\times10^{-9}\,m^2/s)$, $(1.09\,s,\ 7.72\times10^{-10}\,m^2/s)$, and a Jensen distance of 0.50. For the MADCO approach, a total of $N = 35$ acquisitions (a 1D T_1 experiment with 24 inversion times, a 1D diffusion experiment with 10 b-values, and a single 2D acquisition, similar to Fig. 1B) were sufficient to reconstruct an accurate $T_1{-}D$ distribution, with geometric mean peaks of $(0.34\,s,\ 1.88\times10^{-9}\,m^2/s)$, $(1.08\,s,\ 7.74\times10^{-10}\,m^2/s)$, and a Jensen distance of 0.49 from the ground truth. In this case, using MADCO required ~43 less data than the conventional approach.

The results from the more demanding $T_1{-}D$ distribution (phantom B) are presented in the bottom row of Fig. 3. In this case the conventional approach proved to be less accurate than MADCO, even when the full data set was used, leading to geometric mean peaks of $(0.57\,s,\ 1.11\times10^{-9}\,m^2/s)$, $(1.22\,s,\ 7.05\times10^{-10}\,m^2/s)$, and a Jensen distance of 0.69 from the ground truth. It is fair to assume that additional acquisitions would have improved the accuracy of the conventional approach. Because the full acquisition scan time was ~38 h, practical considerations limited the maximal number of acquisitions. Conversely, applying MADCO led to very good agreement with the ground truth distribution, resulting in geometric mean peaks of $(0.50\,s,\ 1.12\times10^{-9}\,m^2/s)$, $(1.03\,s,\ 7.82\times10^{-10}\,m^2/s)$, and a Jensen distance of 0.47, using only $N = 50$ acquisitions (a 1D T_1 experiment with 24 inversion times, a 1D diffusion experiment with 25 b-values, and a single 2D acquisition, see Fig. 1B). Since the conventional approach underperformed MADCO, it is difficult to establish the true acceleration factor in this case, although it is guaranteed to be greater than $1520/50 \approx 30$.

Remarkably, once the marginal distributions are acquired, a single 2D data point is sufficient to reconstruct the 2D distribution. This result is counterintuitive, however, it is the relative simplicity of the 2D spectrum (two relatively well-separated, delta-function-like peaks) that allows for it. It was shown that when more complex peaks shapes are expected, numerous 2D acquisitions in conjunction with MADCO are required [7].

With the imaging parameters that were used in the phantom study 35/50 acquisitions (for phantom A/B), corresponding to ~50/70 min in scan time, were sufficient for a complete and accurate $D{-}T_1$ distribution mapping using the proposed method. Although this is a phantom study, we intentionally used an IR–DWI–EPI pulse sequence, which can be directly translated to *in vivo* preclinical and clinical studies. It is worth noting that the currently applied gradients of up to 900 mT/m are not allowed in clinical applications. However, the maximal b-value of 6200 s/mm^2 is clinically feasible, and can be achieved by using longer diffusion gradient pulses. The repetition time in this study could have been reduced from 10 s to the widely used range in *in vivo* T_1 mapping applications of ~3 s [12], resulting in a total acquisition time of ~16/23 min. Further acceleration can be achieved by using a version of the Look-Locker acquisition [13].

5. Conclusion

The potential impact of this work is directed towards preclinical and clinical applications, where it would allow a comprehensive investigation of compartments and their exchange in a practicable time frame by using the MADCO method in conjunction with a variety of 2D MRI experiments, such as $D{-}T_2$ and $T_1{-}T_2$ correlation and $T_2{-}T_2$ and $D{-}D$ exchange studies. Currently invisible compartments and inaccessible biological processes that may be implicated in neuroplasticity and learning, in normal and abnormal development, and following disease or neurodegenerative conditions and injury. Furthermore, our work may be extended beyond 2D to higher dimensions since the main limitation of experimental time is now relaxed.

Acknowledgements

This work was supported by funds provided by the Intramural Research Program of *The Eunice Kennedy Shriver* National Institute of Child Health and Human Development (NICHD) (ZIA-HD000266).

References

[1] M.D. Does, J.C. Gore, Compartmental study of T1 and T2 in rat brain and trigeminal nerve in vivo, Magn. Reson. Med. 47 (2002) 274–283.
[2] M.D. Hürlimann, L. Burcaw, Y.-Q. Song, Quantitative characterization of food products by two-dimensional D? and ? distribution functions in a static gradient, J. Colloid Interface Sci. 297 (2006) 303–311.
[3] A.E. English, K.P. Whittall, M.L.G. Joy, R.M. Henkelman, Quantitative two-dimensional time correlation relaxometry, Magn. Reson. Med. 22 (1991) 425–434.
[4] J.G. McWhirter, E.R. Pike, On the numerical inversion of the Laplace transform and similar Fredholm integral equations of the first kind, J. Phys. A Math. General 11 (1978) 1729–1745.
[5] L. Venkataramanan, Yi-Qiao Song, M. Hurlimann, Solving Fredholm integrals of the first kind with tensor product structure in 2 and 2.5 dimensions, IEEE Trans. Signal Process. 50 (2002) 1017–1026.
[6] A. Cloninger, W. Czaja, R. Bai, P.J. Basser, Solving 2D Fredholm integral from incomplete measurements using compressive sensing, SIAM J. Imaging Sci. 7 (2014) 1775–1798.
[7] D. Benjamini, P.J. Basser, Use of marginal distributions constrained optimization (MADCO) for accelerated 2D MRI relaxometry and diffusometry, J. Magn. Reson. 271 (2016) 40–45.
[8] D. Benjamini, P.J. Basser, Joint radius-length distribution as a measure of anisotropic pore eccentricity: an experimental and analytical framework, J. Chem. Phys. 141 (2014) 214202.
[9] E. Fordham, A. Sezginer, L. Hall, Imaging multiexponential relaxation in the (y, LogeT1) plane, with application to clay filtration in rock cores, J. Magn. Reson. Ser. A 113 (1995) 139–150.
[10] R. Tibshirani, Regression shrinkage and selection via the lasso, J. the R. Stat. Soc. Ser. B Methodol. 58 (1996) 267–288.
[11] D. Endres, J. Schindelin, A new metric for probability distributions, IEEE Trans. Inf. Theory 49 (2003) 1858–1860.
[12] R.V. Mulkern, H.P. Zengingonul, R.L. Robertson, P. Bogner, K.H. Zou, H. Gudbjartsson, C.R. Guttmann, D. Holtzman, W. Kyriakos, F.A. Jolesz, S.E. Maier, Multi-component apparent diffusion coefficients in human brain: relationship to spin-lattice relaxation, Magn. Reson. Med. 44 (2000) 292–300.
[13] D.C. Look, D.R. Locker, Time saving in measurement of NMR and EPR relaxation times, Rev. Sci. Instrum. 41 (1970) 250.